catalysts

MDPI

Article

Combustion Kinetics of Building Timber Organic Solid Waste

Xin Wang [1], Weichao Xu [1,2,3], Fan Yang [1,2,3], Chunqing Li [4] and Ankang Kan [5,*]

[1] School of Art and Design, Guangxi Polytechnic of Construction, Nanning 530007, China; wangxin093379@163.com (X.W.); xu_weichao@126.com (W.X.); nittick@126.com (F.Y.)
[2] Guangxi Institute of Building Research & Design, Nanning 530007, China
[3] Engineering Technology Innovation Center for Quality Assessment, Ministry of Housing and Urban-Rural Development (MOHURD), Nanning 530007, China
[4] School of Architecture and Urban Planning, Beijing University of Civil Engineering and Architecture, No.1, Zhanlanguan Road, Xicheng District, Beijing 100044, China; lichunqing@bucea.edu.cn
[5] Merchant Marine College, Shanghai Maritime University, Shanghai 201306, China
* Correspondence: ankang0537@126.com

Abstract

This work focuses on the combustion characteristics and kinetics of three building timber organic solid wastes (BTOSW)—China fir, Eucalyptus wood, and Pine wood—aiming to provide theoretical and data support for the thermal conversion and energy utilization of construction-derived woody biomass. Thermogravimetric analysis (TGA) reveals that all three materials exhibit two-stage combustion behavior: volatile combustion at low temperatures (<320 °C) and char combustion at high temperatures (320–500 °C). Increasing the heating rate shifts the decomposition peaks to higher temperature zones, reflecting the combined effects of thermal lag and shortened reaction time. Kinetic analysis shows that the correlation coefficients (R^2) calculated by different models are all greater than 0.97, with the first-order chemical reaction model (O1) demonstrating the highest goodness-of-fit for Pine wood (R^2 = 1.000) and Eucalyptus wood (R^2 = 0.995), indicating that homogeneous chemical reactions dominate the combustion process. The initial combustion temperatures of China fir, Eucalyptus wood, and Pine wood are 256 °C, 262 °C, and 270.9 °C, respectively, with flammability indices of 1.08, 1.46, and 1.15 and comprehensive combustion characteristic indices of 2.71 × 10^{-2}, 1.26 × 10^{-2}, and 1.75 × 10^{-2} °$C^{-2}$$min^{-1}$, respectively. This work provides important theoretical support for both the energy utilization of timber-framed buildings waste and the fire protection design and flame retardancy of timber-framed buildings, contributing to the development of scientific fire prevention measures and the preservation of this architectural heritage.

Keywords: building timber organic solid waste; combustion; TGA; Coats–Redfern

Check for updates

Academic Editor: Patrick Da Costa

Received: 19 December 2025
Revised: 19 July 2026
Accepted: 22 July 2026
Published: 29 July 2026

Copyright: © 2026 by the authors. Licensee MDPI, Basel, Switzerland. This article is an open access article distributed under the terms and conditions of the Creative Commons Attribution (CC BY) license.

1. Introduction

Building timber solid wastes (BTOSW) represent a promising renewable energy alternative with significantly reduced environmental impacts compared to conventional fossil fuels, particularly due to the carbon-neutral nature of biogenic CO_2 emissions during combustion [1–6]. The substitution of fossil-derived fuels with BTOSW could substantially mitigate anthropogenic environmental pollution. Nevertheless, the thermochemical conversion and practical utilization of BTOSW face several technical challenges stemming from their inherent physicochemical characteristics. These include low mass and volumetric energy density, elevated oxygen and moisture content, and heterogeneous and inconsis-

tent material composition [7]. Such properties pose considerable difficulties in terms of feedstock logistics, storage stability, and processing efficiency in energy conversion systems.

Kinetic investigations play a crucial role in elucidating the thermal decomposition behavior of building timber solid wastes (BTOSW) during combustion. Among the various kinetic modeling approaches, the Distributed Activation Energy Model (DAEM) and the Coats–Redfern method are widely employed for such analyses. The DAEM is a multi-reaction kinetic model based on the assumption that thermal decomposition occurs through a series of parallel, independent first-order reactions, each characterized by a distinct organic solid wastes through combustion. activation energy. This distribution reflects the heterogeneity of bond strengths in complex organic materials. DAEM has been extensively applied to study the pyrolysis and combustion kinetics of coal, biomass, and waste-derived fuels, providing insights into the variation of activation energy with conversion extent and temperature [8,9]. Alternatively, the Coats–Redfern method, derived from the Arrhenius equation, is a model-fitting approach used to identify the most probable reaction mechanism governing solid fuel decomposition. This method is typically applied under non-isothermal conditions, allowing for the determination of the apparent activation energy across a defined temperature range [10–12]. Such kinetic analyses are essential for optimizing combustion processes and improving the efficiency of BTOSW thermal conversion.

This study investigated the combustion kinetics of three representative BTOSWs using thermogravimetric analysis (TGA) at multiple heating rates. The Coats–Redfern method was employed to determine kinetic parameters and compare reaction mechanisms. Special emphasis was placed on elucidating the distinct combustion characteristics arising from variations in feedstock composition. This work provides important theoretical support for the energy utilization of building timber.

2. Results

2.1. Combustion Behavior of Raw Materials

The proximate and ultimate analyses are shown in Table 1. Regarding the similarity of ultimate analysis data, the elemental compositions of the three wood species are consistent with published ranges for woody biomass. Extensive literature demonstrates that lignocellulosic biomass from different wood species exhibits remarkably similar ultimate analysis ranges: carbon content typically 46–52% [13,14], hydrogen 5–7% [15], oxygen 40–50% [16], and nitrogen < 0.5% for softwoods [17]. Mosiori et al. [18] reported carbon contents of 40.45–48.88% for six biomass fuels including *Pinus caribaea* and *Eucalyptus grandis*, while the National Renewable Energy Laboratory documented hydrogen contents of 5.87–6.17% for various biomass feedstocks [19]. Our values (C: 46.4–48.0%, H: 6.0–6.1%, O: 45.5–45.9%, N: 0.1–2.2%) fall well within these established ranges, confirming their representativeness.

Table 1. Proximate and ultimate analysis of BTOSWs.

Samples	Proximate Analysis (wt.%)			Ultimate Analysis (wt.%, daf)				HHV (MJ/kg, db)
	A_{ad}	V_{daf}	FC_{daf}	C	H	O	N	
China fir	2.2	78.2	19.6	46.5	6.0	45.9	1.6	16.1
Eucalyptus wood	3.1	78.8	18.1	46.4	6.0	45.5	2.2	16.1
Pine wood	1.4	76.5	22.1	48.0	6.1	45.8	0.1	16.7

Regarding the HHV difference (16.1 vs. 16.7 MJ/kg), the 0.6 MJ/kg variation is both meaningful and within expected interspecies variability. Published HHV ranges for woody biomass typically span 3–5 MJ/kg across different species [20,21]. Vassilev et al. [22] reported HHV ranges of 14–23 MJ/kg for various biomass types, while Mosiori et al. [18] documented variations of up to 1.61 MJ/kg among softwood species from the same region due to growth conditions. The comprehensive database by Sharma et al. [23] showed HHV values ranging from 15.52 to 18.23 MJ/kg for different biomass feedstocks. Our observed 0.6 MJ/kg difference (approximately 3.6% relative difference) therefore reflects genuine compositional variations between species and is scientifically meaningful.

The TG and DTG curves of the BTOSW are shown in Figures 1 and 2. The combustion of BTOSWs included two different stages: volatile combustion at a temperature below 320 °C (Stage 1) and char combustion at 320–350 °C (Stage 2) [24]. During volatile combustion, a shoulder peak was noticed at 215–320 °C, which is attributed to the combustion of hemicellulose, and the peak at 320–500 °C correlated to the combustion of cellulose and lignin. The peak for the volatile combustion stage is significantly larger than that of the char combustion stage because of the high volatile content in the BTOSW sample, as shown in Table 2. In addition, Figures 1 and 2 show that the combustion peaks shifted to higher temperatures as the heating rate increased for all samples. This is due to the poor thermal conductivity of the sample as well as shorter residence times for the decomposition under a higher heating rate.

The combustion characteristic parameters derived from TG data, including the maximum weight loss rate (DTG_{max}), corresponding maximum temperature (T_{max}), initial weight loss temperature (T_i), and final weight loss temperature (T_f) for China fir, Eucalyptus wood, and Pine wood, are presented in Table 2. Analysis of the combustion parameters demonstrated notable interspecies differences in thermal behavior. China fir displayed superior combustibility with the lowest ignition temperature (256 °C at 5 °C/min) and highest comprehensive combustion index (2.71×10^{-2} °$C^{-2}min^{-1}$), while Pine wood exhibited greater thermal stability with consistently higher characteristic temperatures across all heating rates. All samples showed positive correlations between heating rate (5–20 °C/min) and characteristic temperatures, with China fir, Eucalyptus, and Pine wood exhibiting temperature increases of 17.1 °C, 4.1 °C, and 16.3 °C in ignition temperature (Ti), respectively. This heating-rate dependence primarily resulted from thermal lag effects and reduced residence times at reaction zones.

The maximum mass loss rates (DTG_{max}) varied significantly among samples, with China fir showing the most stable char oxidation behavior. The ratio of volatile to char combustion rates ($v_{max,1}/v_{max,2}$) ranged from 2.1 for Pine wood to 3.8 for China fir, suggesting fundamental differences in their thermal decomposition pathways. These combustion characteristics were strongly influenced by the intrinsic properties of each wood species, particularly their hemicellulose/cellulose ratios and lignin aromaticity, which collectively governed both the volatile release patterns and subsequent char oxidation behavior.

The C_b, G, and S_n are flammability index, ignition index, and comprehensive combustion characteristic index. The C_b, G, and S_n are in °C^{-2}·min^{-1}; The R_v is in K^{-2}·min^{-1}.

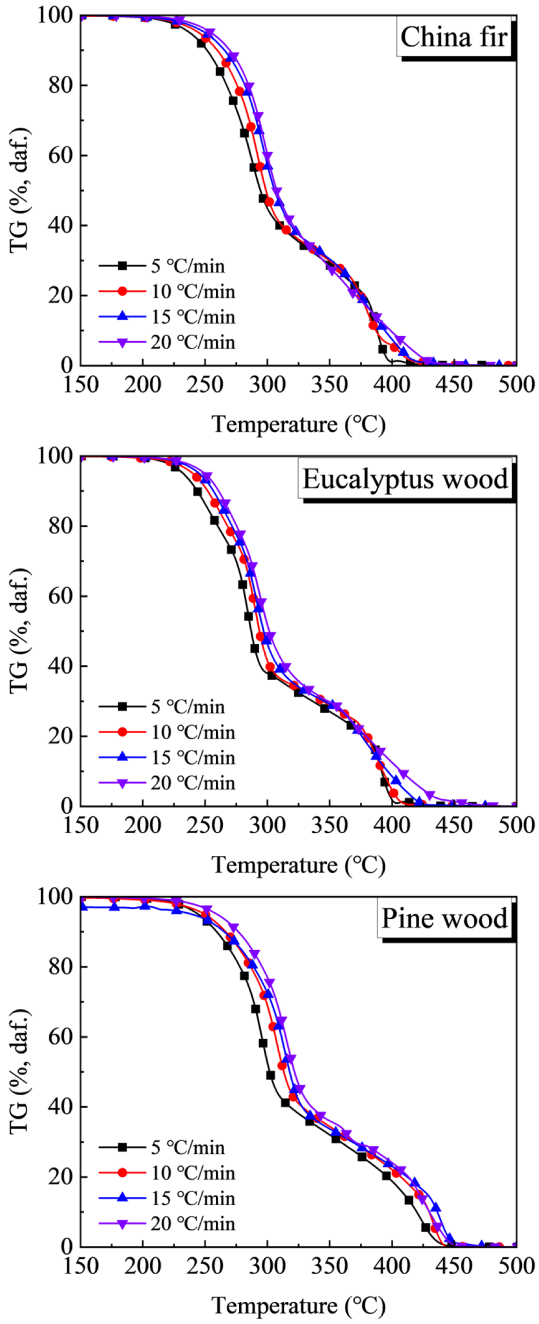


Figure 1. TGA curves of China fir, Eucalyptus wood and Pine wood.

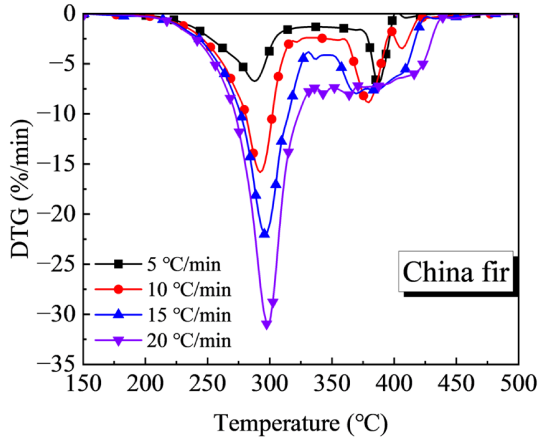


Figure 2. *Cont.*

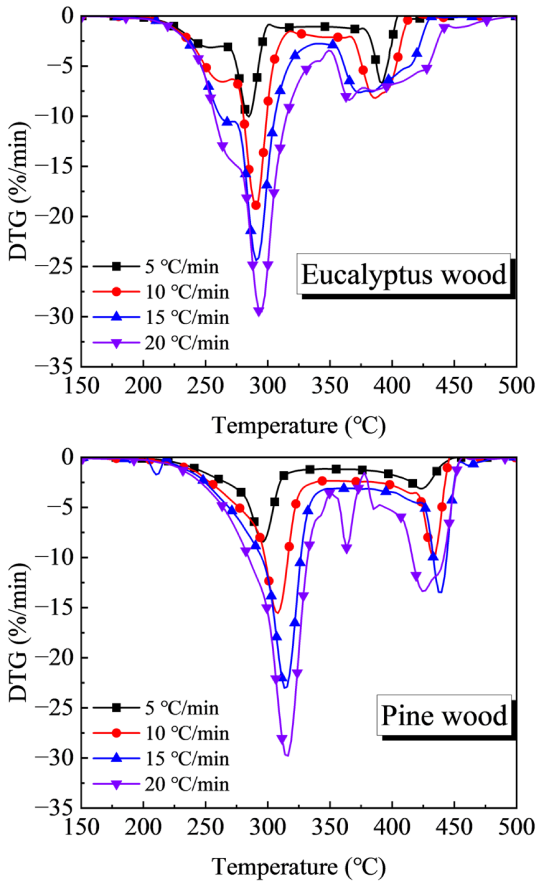


Figure 2. DTG curves of China fir, Eucalyptus wood and Pine wood.

Table 2. Combustion characteristic temperature of three types of biomass.

Heating Rate	T_i	T_f	$T_{max,1}$	$T_{max,2}$	$v_{max,1}$	v_{mean}	$v_{max,2}$	C_b	G	R_v	S_n
°C/min	°C				%/min				$\times 10^4$		$\times 10^2$
China fir											
5	256.0	443.5	287.6	387.4	6.73	2.35	7.07	1.08	0.62	0.81	2.71
10	265.0	459.1	292.3	397.5	15.83	4.43	8.86	2.25	1.30	10.25	1.02
15	270.5	481.5	295.6	369.5	22.01	6.17	7.98	3.01	1.69	15.42	0.72
20	273.1	495.7	297.5	363.8	30.96	7.85	8.09	4.15	2.29	22.24	0.45
Eucalyptus wood											
5	262.1	445.0	284.9	392.4	10.06	2.16	6.68	1.46	0.86	7.91	1.26
10	265.1	475.5	290.5	368.9	18.88	3.85	8.18	2.69	1.50	13.19	0.60
15	265.2	485.1	290.6	372.5	24.40	5.72	7.63	3.47	1.90	17.04	0.53
20	266.2	493.1	295.2	365.4	29.52	7.58	8.41	4.17	2.25	17.91	0.47
Pine wood											
5	270.9	467.5	296.5	422.6	8.42	2.14	3.12	1.15	0.66	5.77	1.75
10	279.3	480.7	308.2	432.6	15.56	4.14	9.97	1.99	1.16	9.26	0.99
15	283.8	485.3	313.4	439.7	23.02	6.08	13.47	2.86	1.67	13.26	0.67
20	287.2	493.3	316.4	424.3	29.78	8.16	13.37	3.61	2.10	17.30	0.54

2.2. Kinetic Analysis

Kinetic modeling of China fir, Eucalyptus wood, and Pine wood combustion was performed using the Coats–Redfern method, evaluating multiple reaction mechanisms to determine the dominant decomposition pathways. The analysis focused on comparing the first-order chemical reaction model (O1), phase-boundary-controlled models (R2, R3), and

diffusion-controlled models (D1–D4) based on their correlation coefficients (R^2), activation energy (E), and mechanistic plausibility.

All models exhibited high R^2 values (>0.97, Table 3), indicating consistent linearity between $ln[g(x)/T^2]$ and $1/T$ across the temperature range. However, the first-order model (O1) demonstrated superior R^2 for Pine wood (1.000) and Eucalyptus wood (0.995), suggesting a stronger fit for homogeneous surface reactions. In contrast, diffusion models (D1–D4) showed marginally lower R^2 for China fir (0.975–0.990), possibly due to its higher volatile content facilitating rapid, less diffusion-limited combustion.

Table 3. Kinetic parameters of China fir, Eucalyptus wood and Pine wood.

Samples	Models	E (kJ/mol)	A (S^{-1})	R^2
China fir	O1	70	1.2×10^6	0.990
	R2	62	4.0×10^4	0.980
	R3	64	6.5×10^4	0.970
	D1	120	1.2×10^{12}	0.975
	D2	130	1.3×10^{13}	0.985
	D3	140	3.5×10^{13}	0.990
	D4	135	3.6×10^{12}	0.988
	Average of D1–D4	131	-	-
Eucalyptus wood	O1	75	8.0×10^8	0.995
	R2	68	1.4×10^7	0.990
	R3	70	2.5×10^7	0.985
	D1	135	1.4×10^{12}	0.980
	D2	145	3.2×10^{13}	0.992
	D3	155	8.8×10^{13}	0.976
	D4	150	3.4×10^{12}	0.982
	Average of D1–D4	146	-	-
Pine wood	O1	95	8.8×10^8	1.000
	R2	88	1.6×10^7	0.999
	R3	92	2.9×10^7	0.996
	D1	160	1.65×10^{12}	0.993
	D2	170	8.0×10^{11}	0.997
	D3	185	2.9×10^{14}	0.984
	D4	180	1.55×10^{12}	0.985
	Average of D1–D4	173	-	-

The O1-derived E values (70–95 kJ/mol) were lower than those from diffusion models, reflecting the energy required for unimolecular bond cleavage in volatile matter. Pine wood's higher E (95 kJ/mol) correlates with its dense lignin network and high cellulose crystallinity (40.5%, Figure 3), which hinder the accessibility of reaction sites. China fir's lower E (70 kJ/mol) aligns with its hemicellulose-rich composition and favorable ash characteristics, promoting facile thermal decomposition, while its crystallinity (39.2%) is intermediate among the three species tested.

Diffusion-controlled E values (103–173) kJ/mol, averaged over D1–D4, were consistently higher, indicating the influence of oxygen transport or ash layer resistance during char combustion. Pine wood's elevated E (173 kJ/mol) suggests its char forms a more compact structure, impeding gas–solid contact, whereas China fir's porous char (due to higher volatile content) reduces diffusion barriers, leading to lower E (131 kJ/mol).

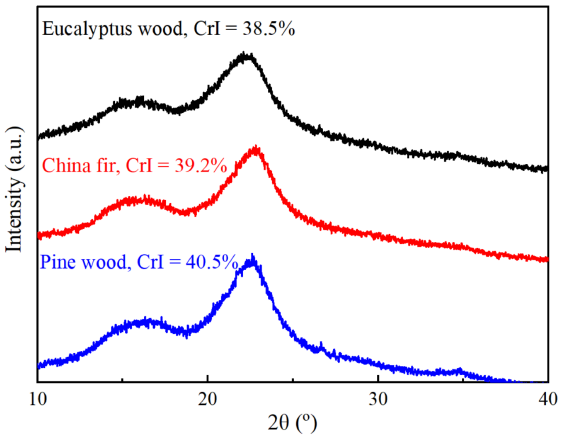


Figure 3. The XRD of China fir, Eucalyptus wood and Pine wood.

The first-order chemical reaction model (O1) provides the most suitable kinetic model for describing BTOSW combustion. The activation energies of the China fir, Eucalyptus wood and Pine wood were 70 kJ/mol, 75 kJ/mol and 95 kJ/mol. Nevertheless, the selection of O1 is supported by literature precedent. Lin et al. [25] employed first-order kinetic models for multi-stage combustion of natural wood species, while Banagiri et al. [26] developed a reduced wood pyrolysis mechanism consisting of three parallel first-order reactions. Jia [10] also applied the first-order reaction equation directly in the Coats–Redfern method to derive kinetic parameters for biomass pellet combustion in stages. These studies collectively demonstrate that the O1 model is a reasonable practical choice for describing the overall combustion kinetics of woody biomass, even though it should not be over-interpreted as a unique mechanistic determination.

Lin et al. [25] systematically investigated four natural wood species and reported activation energies of 85–110 kJ/mol, with pine exhibiting higher values due to its dense lignin structure, corroborating our finding that Pine wood (95 kJ/mol) requires the highest activation energy among the three species tested. Our observation that decomposition peaks shift to higher temperatures with increased heating rates aligns with Ajimotokan et al. [27], who confirmed thermal lag as a universal characteristic in biomass combustion at higher heating rates. Banagiri et al. [26] developed a reduced wood pyrolysis mechanism comprising three parallel first-order reactions, supporting our selection of the first-order model (O1) as the most appropriate for describing biomass combustion. Liu et al. [28] demonstrated that aromaticity and H/C atomic ratios are significantly correlated with combustion reactivity, while Zhang et al. [29] showed that oxidative torrefaction disrupts cellulose crystallinity and lowers pyrolysis initiation temperatures.

2.3. Chemical Property

The chemical properties and crystalline structures of the BTOSW samples were analyzed to correlate with their combustion behaviors and kinetic parameters. Figure 3 shows that the crystallinity of Eucalyptus wood was 38.5%, which was lower than that of China fir and Pine wood (39.2% and 40.5%, respectively). This indicates that the cellulose content in Eucalyptus wood is lower than that in Chinese fir and Pine wood. Cellulose crystallinity directly influences the accessibility of biomass to thermal decomposition. Lower CrI values indicate a higher proportion of amorphous cellulose, which is more readily degraded during combustion. Eucalyptus wood's lowest CrI (38.5%) suggests enhanced reactivity due to its disordered cellulose structure, aligning with its moderate activation energy (75.0 kJ/mol, Table 3) and intermediate combustibility. Conversely, Pine wood's high CrI (40.5%) reflects tightly packed cellulose fibrils, stabilized by lignin cross-linking, which increases the energy barrier for bond cleavage (95.0 kJ/mol, Table 3) and results in lower flammability.

XRD analysis revealed marginal differences in cellulose crystallinity (38.5–40.5%) among the three species. While crystallinity may partially influence combustion behavior, the superior combustibility of China fir cannot be attributed solely to this factor, as Eucalyptus wood actually exhibited the lowest crystallinity. The observed differences in combustion performance likely result from combined effects of crystallinity, ash composition, lignin content, and hemicellulose-to-cellulose ratio. First, the inorganic constituents present in biomass ash—particularly K, Ca, Mg, and Si—are known to significantly influence combustion behavior [30,31]. Wood ash typically contains 0.2–1.7% of dry weight, with potassium and calcium oxides comprising over 50% of total ash content; these elements can catalyze oxidation reactions and affect ignition temperatures [32]. The proximate analysis (Table 1) shows different ash contents (China fir: 2.2%, Eucalyptus: 3.1%, Pine: 1.4%), suggesting varying inorganic compositions that may contribute to the observed differences in combustion performance. For instance, the higher ash content in Eucalyptus wood (3.1%) may influence its intermediate combustion behavior. Second, beyond crystallinity, the aromaticity and cross-linking density of lignin significantly affect thermal stability. Pine wood's higher lignin content likely contributes to its elevated activation energy (95 kJ/mol) through the formation of more stable char structures [31]. Third, the ratio of hemicellulose to cellulose influences volatile release patterns, with hemicellulose decomposing at lower temperatures (215–320 °C) and contributing to the shoulder peaks observed in DTG curves [25]. We acknowledge that without detailed ash compositional analysis, the precise role of inorganic elements cannot be definitively established. Future work should include comprehensive ash analysis (e.g., XRF or ICP-MS) to quantify K, Ca, Mg, Si, and other elements, enabling a more complete understanding of the structure–property relationships governing BTOSW combustion.

3. Materials and Methods

3.1. Materials

Three BTOSWs—China fir, Eucalyptus wood and Pine wood—were selected as raw materials for this study. The samples were mechanically crushed and sieved to a particle size fraction of 40–60 mesh (250–425 μm) to minimize internal temperature gradients during thermal analysis. The HHV of BTOSWs was calculated based on elemental composition according to Dulong's equation [24].

3.2. Combustion

The combustion behavior of China fir, Eucalyptus wood and Pine wood was investigated using a thermogravimetric analyzer (TGA). Experiments were conducted under an oxidative atmosphere (20.0% O_2 and 80.0% N_2) with a carrier gas flow rate of 100 mL min^{-1}. Approximately 10 mg of each sample was heated from 25 °C to 500 °C. To ensure reproducibility, all tests were performed in triplicate.

3.3. Characterization

Proximate analysis of BTOSWs was performed following the Chinese National Standard (GB/T 28731-2012). Ultimate analysis was conducted using an Elementar Vario EL-2 elemental analyzer (Elementar, Langenselbold, Germany). The crystalline structure of the samples was examined by X-ray diffraction (XRD; PANalytical X'Pert PRO, Almelo, The Netherlands).

3.4. Kinetic Study

The kinetic parameters of biomass combustion were determined using the Coats–Redfern method. The Coats–Redfern method was employed as follows [33]:

$$ln\left[\frac{g(X)}{T^2}\right] = ln\left[\frac{AR}{\beta E}\left(1-\frac{2RT}{E}\right)\right] - \frac{E}{RT} \quad (1)$$

For typical combustion temperatures (25–500 °C), the term $ln\left[\frac{AR}{\beta E}\left(1-\frac{2RT}{E}\right)\right]$ remains approximately constant [34,35]. The value of E can be acquired via the slope, and the pre-exponential factor (A) can be attained by using the intercept of Equation (2) [36,37].

$$k = Aexp\left(\frac{-E}{RT}\right) \quad (2)$$

The appropriate reaction mechanism model ($g(x)$) was selected from Table 4, which includes common solid-state reaction models. The Homogeneous Model (HM) assumes uniform reactions throughout the BTOSW. Some theoretical details are available in published studies [24].

Table 4. The f(x) and g(x) functions for the kinetic model.

Model	Symbol	*f(x)*	*g(x)*
Chemical reaction (HM)			
First-order	O_1	$(1-x)$	$-\ln(1-x)$
Phase boundary-controlled reactions or shrinking core model (SCM)			
Two dimensions (Contracting Cylinder)	R2	$2(1-x)^{1/2}$	$1-(1-x)^{1/2}$
Three dimensions (Contracting Sphere)	R3	$3(1-x)^{2/3}$	$1-(1-x)^{1/3}$
Dimensional diffusion models			
One-dimensional	D1	$\alpha^{-1}/2$	α^2
Two-dimensional, cylindrical symmetry	D2	$[-\ln(1-\alpha)]^{-1}$	$\alpha+(1-\alpha)\ln(1-\alpha)$
Three-dimensional, spherical symmetry	D3	$3(1-\alpha)^{2/3}[1-(1-\alpha)^{1/3}]^{-1/2}$	$[1-(1-\alpha)^{1/3}]^2$
Three-dimensional, cylindrical symmetry	D4	$(1-2\alpha/3)-(1-a)^{2/3}$	$(1-2\alpha/3)-(1-a)^{2/3}$

4. Conclusions

This study systematically investigated the combustion characteristics and kinetics of three representative building timber organic solid wastes (BTOSW)—China fir, Eucalyptus wood, and Pine wood—using thermogravimetric analysis and the Coats–Redfern method. The following conclusions can be drawn:

1. All three BTOSW exhibited two-stage combustion, comprising volatile combustion below 320 °C and char combustion between 320 and 500 °C. Increasing heating rates from 5 to 20 °C/min shifted all characteristic temperatures to higher zones due to thermal lag effects, with ignition temperature increases of 17.1 °C, 4.1 °C, and 16.3 °C for China fir, Eucalyptus wood, and Pine wood, respectively.
2. China fir demonstrated the best combustibility with the lowest ignition temperature (256 °C at 5 °C/min) and highest comprehensive combustion characteristic index (2.71×10^{-2} °C^{-2}min^{-1}), while Pine wood exhibited the greatest thermal stability with consistently higher characteristic temperatures across all heating rates.
3. The first-order chemical reaction model (O1) provided the best fit for all samples (R^2 = 0.990–1.000), indicating that homogeneous chemical reactions dominate the combustion process. Activation energies followed the order China fir (70 kJ/mol) < Eu-

calyptus wood (75 kJ/mol) < Pine wood (95 kJ/mol), correlating positively with thermal stability.

4. These findings provide essential kinetic parameters and mechanistic insights for optimizing combustion systems, designing biomass-fired boilers, and developing energy recovery strategies from construction and demolition wood wastes. Moreover, they provide theoretical references for the fire protection design and flame-retardant treatment of timber-framed buildings, which is of great significance for formulating effective fire prevention strategies and preserving cultural heritage. The correlation between structural properties and combustion behavior offers a basis for feedstock selection and pretreatment optimization.

This study was conducted under controlled laboratory conditions using small sample sizes and may not fully represent large-scale combustion behavior. Future work should investigate the combustion kinetics under industrially relevant conditions, explore co-combustion with other feedstocks, and examine the evolution of gaseous pollutants during combustion.

Author Contributions: X.W. (Xin Wang): Writing—original draft, Writing—review and editing; W.X. (Weichao Xu) and F.Y. (Fan Yang): Investigation, Visualization, Methodology; C.L. (Chunqing Li): Resources, Supervision; A.K. (Ankang Kan): Investigation, Formal analysis, Writing—original draft, Writing—review and editing, Supervision. All authors have read and agreed to the published version of the manuscript.

Funding: This work was supported by the 2024 Guangxi Colleges and Universities Young and Middle-aged Teachers' Scientific Research Basic Ability Promotion Project (2024KY1192) and by the 2020 Special Fund Subsidy Project for Energy-Saving and Emission-Reduction (Building Energy-Saving) of Guangxi Zhuang Autonomous Region.

Data Availability Statement: The data supporting the findings of this study are included within the article. Additional data are available from the corresponding author upon reasonable request.

Conflicts of Interest: The authors declare no conflicts of interest.

References

1. Zanzi, R.; Sjöström, K.; Björnbom, E. Rapid high-temperature pyrolysis of biomass in a free-fall reactor. *Fuel* **1996**, *75*, 545–550. [CrossRef]
2. Borah, A.J.; Singh, S.; Goyal, A.; Moholkar, V.S. An assessment of the potential of invasive weeds as multiple feedstocks for biofuel production. *RSC Adv.* **2016**, *6*, 47151–47163. [CrossRef]
3. Chen, J.B.; Wang, Y.H.; Lang, X.M.; Ren, X.; Fan, S. Evaluation of agricultural residues pyrolysis under non-isothermal conditions: Thermal behaviors, kinetics, and thermodynamics. *Bioresour. Technol.* **2017**, *241*, 340–348. [CrossRef] [PubMed]
4. Jia, W.G.; Zhang, H.; Liu, B.C.; Xiao, J.J.; Yang, H.P.; Chen, H.P. Pyrolytic Interactions in Biomass: A Review Across Molecular, Component, and Feedstock Scales. *Energy Fuels* **2025**, *39*, 22463–22488. [CrossRef]
5. Wang, Y.F.; Qin, Y.H.; Vassilev, S.V.; He, C.; Vassileva, C.G.; Wei, Y.X. Migration behavior of chlorine and sulfur during gasification and combustion of biomass and coal. *Biomass Bioenergy* **2024**, *182*, 107080. [CrossRef]
6. Wang, M.H.; Xie, Y.P.; Gao, Y.; Huang, X.H.; Chen, W. Machine learning prediction of higher heating value of biochar based on biomass characteristics and pyrolysis conditions. *Bioresour. Technol.* **2024**, *396*, 130364. [CrossRef] [PubMed]
7. El Bari, H.; Fanezoune, C.K.; Dorneanu, B.; Arellano-Garcia, H.; Majozi, T.; Elhenawy, Y.; Bayssi, O.; Hirt, A.; Peixinho, J.; Dhahak, A.; et al. Catalytic fast pyrolysis of lignocellulosic biomass: Recent advances and comprehensive overview. *J. Anal. Appl. Pyrolysis* **2024**, *177*, 106390. [CrossRef]
8. De Caprariis, B.; Santarelli, M.; Scarsella, M.; Herce, C.; Verdone, N.; De Filippis, P. Kinetic analysis of biomass pyrolysis using a double distributed activation energy model. *J. Therm. Anal. Calorim.* **2015**, *121*, 1403–1410. [CrossRef]
9. Miura, K.; Maki, T. A simple method for estimating f(E) and k(0)(E) in the distributed activation energy model. *Energy Fuel* **1998**, *12*, 864–869. [CrossRef]

10. Jia, G.H. Combustion characteristics and kinetic analysis of biomass pellet fuel using thermogravimetric analysis. *Processes* **2021**, *9*, 868. [CrossRef]
11. Zhang, P.; Chen, Z.Y.; Zhang, Q.L.; Zhang, S.; Ning, X.; Zhou, J. Co-pyrolysis characteristics and kinetics of low metamorphic coal and pine sawdust. *RSC Adv.* **2022**, *12*, 21725–21735. [CrossRef] [PubMed]
12. Sharma, A.; Mohanty, B. Thermal degradation of mango (Mangifera indica) wood sawdust in a nitrogen environment: Characterization, kinetics, reaction mechanism, and thermodynamic analysis. *Rsc Adv.* **2021**, *11*, 13396–13408. [CrossRef] [PubMed]
13. Vassilev, S.V.; Vassileva, C.G.; Vassilev, V.S. Advantages and disadvantages of composition and properties of biomass in comparison with coal: An overview. *Fuel* **2015**, *158*, 330–350. [CrossRef]
14. García, R.; Pizarro, C.; Lavín, A.G.; Bueno, J.L. Characterization of Spanish biomass wastes for energy use. *Bioresour. Technol.* **2012**, *103*, 249–258. [CrossRef] [PubMed]
15. Demirbaş, A. Combustion characteristics of different biomass fuels. *Prog. Energy Combust. Sci.* **2004**, *30*, 219–230. [CrossRef]
16. Sheng, C.; Azevedo, J.L.T. Estimating the higher heating value of biomass fuels from basic analysis data. *Biomass Bioenergy* **2005**, *28*, 499–507. [CrossRef]
17. Jenkins, B.M.; Baxter, L.L.; Miles, T.R., Jr.; Miles, T.R. Combustion properties of biomass. *Fuel Process. Technol.* **1998**, *54*, 17–46. [CrossRef]
18. Mosiori, G.O. Thermo-Chemical Characteristics of Potential Gasifier Fuels in Selected Regions of the Lake Victoria Basin. Master's Thesis, Kenyatta University, Nairobi, Kenya, 2014.
19. Annamalai, K.; Sweeten, J.M.; Mukhtar, S.; Thien, B.; Wei, G.; Priyadarsan, S. *Renewable Energy and Environmental Sustainability Using Biomass From Dairy and Beef Animal Production*; NREL Report No. SR-5100-54427; National Renewable Energy Laboratory: Golden, CO, USA, 2012.
20. McKendry, P. Energy production from biomass (part 1): Overview of biomass. *Bioresour. Technol.* **2002**, *83*, 37–46. [CrossRef] [PubMed]
21. Telmo, C.; Lousada, J. The explained variation by lignin and extractive contents on higher heating value of wood. *Biomass Bioenergy* **2011**, *35*, 1663–1667. [CrossRef]
22. Vassilev, S.V.; Baxter, D.; Andersen, L.K.; Vassileva, C.G. An overview of the chemical composition of biomass. *Fuel* **2010**, *89*, 913–933. [CrossRef]
23. Waziri, S.A.; Dhada, I.; Das, R. A comprehensive database for characterizing potential of common biomass feedstocks. *Biomass Convers. Bior.* **2025**, *15*, 16737–16763. [CrossRef]
24. Nie, Y.; Song, X.; Shan, M.; Yang, X. Effect of pelletization on biomass thermal degradation in combustion: A case study of peanut shell and wood sawdust using macro-TGA. *Energy Built Environ.* **2025**, *5*, 920–926. [CrossRef]
25. Lin, Y.-X.; Wang, Q.; Li, Q.-X.; Lin, Q.-W.; Man, P.-R.; Zhou, S.-N.; Li, Y.; Deng, J. Multi-stage study of pyrolysis kinetics, combustion characteristics, and fire modeling for selected nature wood species. *Fuel* **2026**, *407*, 137296. [CrossRef]
26. Banagiri, S.; Parameswaran, M.; Khadakkar, I.; Meadows, J.; Lattimer, B.Y. A reduced wood pyrolysis mechanism for evaluating solid and gas phase parameters. *Fuel* **2025**, *381*, 133416. [CrossRef]
27. Ajimotokan, H.A.; Saidu, N.S.; Aladodo, M.A.; Oladosu, K.O.; Samuel, O.D.; Abdulrahman, K.O.; El-Suleiman, A.; Salihu, Y.S.; Ajao, K.R. Combustion characteristics of torrefied corncob and African birch wood residues at higher heating rate. *Sci. Afr.* **2025**, *27*, e02494. [CrossRef]
28. Liu, X.; Zou, Q.; Wang, X.; Huang, Y.; Zhang, C.; Yuan, S.; Dai, X. Structure-reactivity insights in combusting rice straw hydrochar: Role of hydrothermal temperature. *Renew. Energy* **2026**, *260*, 125149. [CrossRef]
29. Zhu, L.; Cen, K.; Ni, X.; Liu, M.; Chen, D. Potential of Cellulose After Oxidative Torrefaction for Fuel Enhancement and Utilization: Properties and Pyrolysis Characteristics. *Coatings* **2025**, *15*, 407. [CrossRef]
30. Vassilev, S.V.; Vassileva, C.G.; Song, Y.C.; Li, W.Y.; Feng, J. Ash contents and ash-forming elements of biomass and their significance for solid biofuel combustion. *Fuel* **2017**, *208*, 377–409. [CrossRef]
31. Löffler, G.; Wargadalam, V.J.; Winter, F. Catalytic effect of biomass ash on CO, CH_4 and HCN oxidation under fluidised bed combustor conditions. *Fuel* **2002**, *81*, 711–717. [CrossRef]
32. Dietenberger, M. Update for combustion properties of wood components. *Fire Mater.* **2002**, *26*, 255–267. [CrossRef]
33. Hu, Y.J.; Wang, Z.Q.; Cheng, X.X.; Ma, C. Non-isothermal TGA study on the combustion reaction kinetics and mechanism of low-rank coal char. *RSC Adv.* **2018**, *8*, 22909–22916. [CrossRef] [PubMed]
34. Çepelioğullar, Ö.; Pütün, A.E. Thermal and kinetic behaviors of biomass and plastic wastes in co-pyrolysis. *Energy Convers. Manag.* **2013**, *75*, 263–270. [CrossRef]
35. Cheng, G.; He, P.W.; Xiao, B.; Hu, Z.-Q.; Liu, S.-M.; Zhang, L.-G.; Cai, L. Gasification of biomass micron fuel with oxygen-enriched air: Thermogravimetric analysis and gasification in a cyclone furnace. *Energy* **2012**, *43*, 329–333. [CrossRef]

36. Yan, L.B.; He, B.S.; Hao, T.Y.; Pei, X.; Li, X.; Wang, C.; Duan, Z. Thermogravimetric study on the pressurized hydropyrolysis kinetics of a lignite coal. *Int. J. Hydrogen Energy* **2014**, *39*, 7826–7833. [CrossRef]
37. Edreis, E.; Luo, G.Q.; Li, A.J.; Xu, C.; Yao, H. Synergistic effects and kinetics thermal behaviour of petroleum coke/biomass blends during H_2O co-gasification. *Energy Convers. Manag.* **2014**, *79*, 355–366. [CrossRef]

Disclaimer/Publisher's Note: The statements, opinions and data contained in all publications are solely those of the individual author(s) and contributor(s) and not of MDPI and/or the editor(s). MDPI and/or the editor(s) disclaim responsibility for any injury to people or property resulting from any ideas, methods, instructions or products referred to in the content.